Journal of Materials Chemistry A

Accepted Manuscript

ROYAL SOCIETY OF CHEMISTRY

www.rsc.org/materialsA

Journal Name

ARTICLE

A trimetallic V-Co-Fe oxide nanoparticle as an efficient and stable electrocatalyst for oxygen evolution reaction

Received 00th January 20xx,
Accepted 00th January 20xx

DOI: 10.1039/x0xx00000x

www.rsc.org/

Taotao Gao,[a] Zhaoyu Jin,[b] Mei Liao,[b] Jinlan Xiao, [a] Hongyan Yuan [a] and Dan Xiao*[ab]

Hydrogen (H_2) generated from water splitting is deemed as the ideal replacement for conventional sources of energy. Catalysts play a valuable role in water splitting, especially the oxygen evolution reaction (OER). Here, we report a Fe-doped $Co_3V_2O_8$ nanoparticle catalyst (iron-rich V-Co-Fe), which possesses outstanding OER catalytic activity with $\eta_{j=10\ mA\ cm^{-2}}$ = 307 mV, and a low Tafel slope of 36 mV dec^{-1}, benefiting by large degree of amorphization, rich porous structure as well as high specific surface area (about 232.1 $m^2\ g^{-1}$). And, more remarkable, the catalytic performance of the V-Co-Fe catalyst is markedly superior to commercial ruthenium oxide. In addition, the durability of the V-Co-Fe catalyst is fine. The current density collapses by less than 3 percent at 1.55V *vs.* RHE after 11 h, in comparison with the initial value. Moreover, this work reveals that the V-Co-Fe catalyst displays an excellent performance in both OER catalytic activity and stability, which may have the potential to be the ideal substitute of noble metal-based catalysts for water splitting to obtain affordable clean energy.

Introduction

With the looming of energy crisis, and increasing serious environmental pollution, hydrogen (H_2) generated from water splitting has garnered significant recent attention for its potential for becoming one of primary energy sources with high efficiency and environmental friendliness.[1-4] The oxygen evolution reaction (OER: $4OH^- \leftrightarrow O_2 + 2H_2O + 4e^-$ for alkaline media and $2H_2O \leftrightarrow O_2 + 4H^+ + 4e^-$ for acid media), a critical key of water splitting, recharging metal-air batteries and solar cells, is limited by the sluggish kinetic, which results in a high overpotential for this reaction.[5-10] Thus, the design and preparation of catalysts with high catalytic activity to reduce overpotential become a focus of research.[3, 11, 12] Among a number of previous researches, compounds and oxides of some noble metals are the best catalysts to expedite OER, such as iridium (Ir) and ruthenium (Ru).[13-15] However, one issue suppressing the large-scale application of those catalysts is their high cost, low abundance and inferior durability.[13] Hence, more scientific researches concentrate on the development of oxygen electrode catalysts based on non-noble metals[7, 9, 16, 17] and metal-free materials[10, 18].

Less expensive and more abundant transition metal is proposed to be one of the most promising materials for water splitting. For example, $Co^{(III/IV)}$ centers produced from Co-based catalysts in reaction are important active sites for catalysts towards OER,[19, 20] so a variety of Co-based catalysts with different composition and morphology have been prepared.[15, 21-23] Co_3O_4 nanoparticles display efficient OER catalytic activity resulting from the exposure of more catalytic active sites.[16] In addition, because vanadium has multiple valence state, V-based compounds exhibit excellent electrochemical performance. Man Xing et.al have successfully prepared $Co_3V_2O_8$ that shows considerable OER catalytic activity and good stability, because of high specific surface area.[24] However, vanadium is relatively expensive comparing with other transition metals ($18200-18700 a tonne for V_2O_5), and the damage of vanadium to the environment and human health is rather severe.[25, 26] On the contrary, iron is the most low-cost ($970-1200 a tonne for Fe_2O_3) and abundant transition metal, and its toxicity is substantially lower than vanadium.[27] Meanwhile, iron also has multiple valence state, and has become a highly visible material for OER.[28, 29] Rodney D.L and co-workers have confirmed that proper concentrations (20%-40%) of iron in binary and ternary films can significantly improve the Tafel slopes of catalysts, and the stability of higher oxidation levels of the metals.[28] Additionally, the presence of iron can induce defects formation to obtain high specific surface area and provide more edge sites.[30] During oxygen evolution reaction, those changes may promote the exposure of the catalyst surface to electrolyte and form more surfaces with large degree of amorphous, which will be an effective force for high OER activity.[31, 32] Drawing inspiration from above, we try to synthesis Fe-doped $Co_3V_2O_8$ (a part of vanadium in $Co_3V_2O_8$ lattice are replaced by iron) catalyst, in

[a] College of Chemical Engineering, Sichuan University, Chengdu 610064, P. R. China.
[b] Key Laboratory of Green Chemistry and Technology, Ministry of education, College of Chemistry, Sichuan University, Chengdu 610064, P. R. China. E-mail: xiaodan@scu.edu.cn; Fax: +86-28-85415029; Tel: +86-28-85416029.

† Electronic Supplementary Information (ESI) available: additional XRD spectra, polarization curves, Tafel plots and electrolyte resistance of catalysts prepared in this work, overall XPS spectra, nitrogen adsorption–desorption isotherm and EIS spectra of V-Co-Fe-343, List of relative parameters for oxygen evolution reaction. See DOI: 10.1039/x0xx00000x

order to improve catalytic performance while also reducing vanadium in catalysts.

Here, we prepared iron-rich V-Co-Fe-343 trimetallic oxide nanoparticles in order to replace vanadium in $Co_3V_2O_8$ lattice via a simple and mild hydrothermal method. The doping of iron remarkably improves the electrical conductivity and the Tafel slope of the V-Co-Fe-343 catalyst, which is propitious to enhance the catalytic activity for OER. The V-Co-Fe-343 catalyst just needs a low overpotential of 307 mV to achieve a current density of 10 mA cm^{-2} and has a small Tafel slope of 36mV dec^{-1}. Because of large degree of amorphization, rich porous structure as well as high specific surface area, the V-Co-Fe-343 nanoparticles display an outstanding performance in both OER catalytic activity and stability in alkaline electrolyte. Moreover, the strategy in this work may give a new pathway to design and obtain low-cast, highly active and environmentally friendly OER catalysts.

Experimental section

Synthesis of multiplex metal oxides

Synthesis of multiplex metal oxides was carried out through a two-step process. In the first step, a series of aqueous solution, with different molar ratios of cobalt ($CoSO_4·7H_2O$), iron ($Fe_2(SO_4)_3·XH_2O$) and vanadium ($VOSO_4·3H_2O$). Then, using pH dollars adjust pH by gradually adding ammonia solution (30% in water) to the above solution until pH~10.5, with stirring constantly on a magnetic at room temperature. In the second step, the above mixture was loaded into a 10 mL Teflon-lined stainless steel autoclave and heated at 180 ℃ for 22 h in the oven. When the oven was cooled to room temperature, the product in suspension was separated using a high speed centrifuge, then washed with plenty of distilled water for two times and absolute ethanol for one time, respectively. Next, the collected product was dried at 60 ℃ for 12 h in a vacuum oven. A series of products are labeled as V-Co-Fe-xyz (xyz is the molar ratios of cobalt, iron and vanadium sources).

Characterizations

To investigate the crystallite structures, X–ray diffraction (XRD) patterns were obtained on a Fangyuan DX-1000 powder X-ray diffractometer (China) with Cu Kα radiation at a tube voltage of 40 kV, and the data of 2θ were collected from 20° to 80° range with 0.02° of the step size at the rate of 5° min^{-1}. The surface appearance of the catalysts were observed by scanning electron microscopy (SEM) using a field emission Hitachi S4800 microscope (Japan). The transmission electron microscopy (TEM) and high-resolution transmission electron microscopy (HRTEM) analysis were carried out on a FEI Tecnai G2 F20 S (USA) at 200 kV of an accelerating voltage in order to confirm the size and lattice parameter of the nanoparticles. The specific surface area and the pore-size distribution is calculated by Brunauer–Emmett–Teller (BET) formulations and Barrett–Joyner–Halenda (BJH) method, respectively, according to the N_2 adsorption-desorption experiment, which is performed on a Quadrasorb Nava 4000 Automated Surface Area (Quantachrome, USA).The chemical states of V, Co, Fe and O in nanoparticle catalysts prepared in this work were certified by X–ray photoelectron spectroscopy (XPS) performed on a Kratos AXIS ULTRADLD Photoelectron Spectroscope (UK) with an Mg Kα radiation ($h\nu$ = 1253.6 eV) and the energy resolution is 0.9 eV. All XPS spectra were corrected using the C 1s line at 284.6 eV.

Calculation Method

First-principle calculations were performed by density-functional theory (DFT)[33,34]executed in the CASTEP package.[35] The generalized-gradient approximation (GGA) in the Perdew–Burke–Ernzerhof (PBE)[36] form was employed at 340 eV of a cutoff energy for the plane waves. The geometric optimization was carried out using single cell of $Co_3V_2O_8$ and V-Co-Fe-343 with the crystal plane of (122). The densities of states (DOS) was calculating using a denser k-points grid of 3 × 3 × 3, and the thickness of vacuum space is set to be 15 Å.

Electrochemical measurements

A rotation disk electrode (RDE) was used to carry out electrochemical measurements on an Autolab PGSTAT 12 potentiostat/galvanostat (Metrohm, Switzerland) with a rotation speed of 1600 rpm at room temperature and all tests were performed in 1.0 M KOH electrolyte. The working electrode, reference electrode and counter electrode in this study are a 5mm diameter glassy carbon (GC) electrode, Hg/HgO electrode and graphite electrode, respectively. Because of the presence of electrolyte resistance, the ohmic potential drop (iR, where i is the current and R is the electrolyte resistance.) in this paper were compensated according to the simulation values of the electrochemical impedance spectroscopy (typically ~7.5 Ω for 1 M KOH). In order to conveniently compare with other catalysts reported at different testing conditions, all the values of potential were presented *versus* the reversible hydrogen electrode (RHE) using the calibration equations: $E_{RHE} = E_{Hg/HgO\ vs.\ NHE} + 0.059 \times pH$, and correspond to applied potentials is denoted as E – iR. 5 mg catalyst powder and 10 μL Nafion solution (5% wt, Dupont, USA) were dispersed into a mixed solution, which contains 375 μL distilled water and 125 μL isopropyl alcohol, to prepare catalyst inks used in electrochemical tests. Prior to electrochemical testing, the working electrode was treated as follows: firstly, the glassy carbon electrodes polished using alumina suspension, washed with distilled water and dried by nitrogen. Then 6 μL catalysts inks were dropped onto above glassy carbon electrodes, and wait to nature dry at room temperature. The polarization curves of the catalysts were collected by linear sweep voltammetry (LSV) from 0 to 0.8 V *vs.* Hg/HgO at 10 mV s^{-1} of a scan rate. For pressing closer to the actual application, the catalytic stability and Faradaic efficiency of the catalysts were characterized using carbon fiber paper covered with catalysts as the working electrode. The

electrochemical impedance spectra (EIS) of those catalysts were characterized on the glassy carbon electrode and carbon fiber paper, respectively. The Faradaic efficiency of catalysts was investigated using a PASCO O_2 sensing device (USA).

Results and discussion

The X-ray diffraction (XRD) patterns of catalysts obtained in this work are presented in Fig. 1a and Fig. S1. As shown in Fig. 1a and Fig. S1, the patterns of $Co_3V_2O_8$ and $(CoFe_2)O_4$ are coincide well with the standard patterns for $Co_3V_2O_8$ (JCPDS no. 074-1487) and $(CoFe_2)O_4$ (JCPDS no. 079-1744), respectively. The tiny differences of angle of characteristic peaks for those two samples suggest that they have the closed distance of the crystal plane (d). Meanwhile, the $Fe^{(III)}$ ion radius (0.055 nm) is close to that of $V^{(V)}$ (0.054 nm). These features make it possible that $Fe^{(III)}$ ions dissolve into the $Co_3V_2O_8$ lattice, and replace a part of $V^{(V)}$ to form Fe-doped $Co_3V_2O_8$ sample with lattice defects.[37, 38] With regard to the V-Co-Fe-343 sample, the diffraction pattern shows apparent diffraction peaks for $Co_3V_2O_8$, along with SAED patterns (Fig. S2, inset), but the diffraction peaks has little shift, and some peaks become weakly and all but disappearing, which could be due to the iron doping in $Co_3V_2O_8$ lattice and replacing a part of vanadium to form lattice defects.[37] This also can be proved by the corresponding simulated XRD patterns about the Fe-doped $Co_3V_2O_8$. In addition, the peaks of the V-Co-Fe-343 are weaker for diffraction intensity and broader for peak width, as shown in Fig. 1a, which indicates its large degree of amorphization, lower crystallinity and smaller particle size, and this is proved by SEM and TEM images (Fig. 1b and 1c). Those characteristics are good for the forming of more transportation channels and the exposure of catalytic active sites in catalysts.[17, 24]

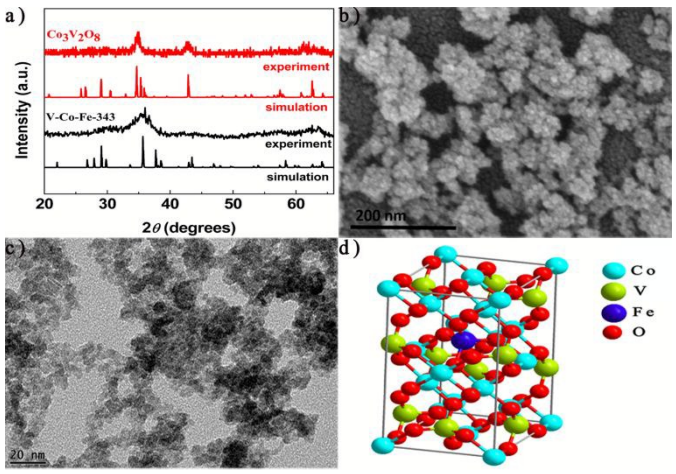

Fig1. a) XRD patterns of $Co_3V_2O_8$ and the V-Co-Fe-343 obtained in this work, the simulated patterns of Fe-doped $Co_3V_2O_8$ with 1% vandium replaced by iron; b) high-magnification SEM image, c) TEM and c) HRTEM images d) The schematic crystal structure of Fe-doped $Co_3V_2O_8$ (V-Co-Fe-343) according to that of $Co_3V_2O_8$.

The SEM image presented in Fig. 1b shows that V-Co-Fe-343 has an interesting morphology that lots of small nanoparticles irregularly to form many bigger nanoparticles with different sizes. To future observe the V-Co-Fe-343 nanoparticles, TEM is applied in our work. As shown in Fig. 1c, many size similar nanoparticles comprise the V-Co-Fe-343, and the size of small nanoparticles is around 6-8 nm according to High-resolution TEM image (Fig. S2). In addition, because the specific surface area and distribution of pore size affect the electrocatalytic performance markedly,[16] it is necessary to carry out BET measurement. Fig. S3 describes the N_2 adsorption-desorption isotherm and distribution of pore size of the obtained V-Co-Fe-343, respectively, using $Co_3V_2O_8$ obtained in this work for reference sample. As shown in Fig. S3a, the formation of typical type IV hysteresis loops reveals the existence of mesoporous structure in these two samples,[39, 40] which is further proved by the distribution of pore size for the obtained V-Co-Fe-343 and $Co_3V_2O_8$ sample, at 3.7 nm and 6.4nm (Fig. S3b and inset), respectively. But, the specific surface area of the V-Co-Fe-343 sample is about 232.1 $m^2\ g^{-1}$, which is significantly higher than the bimetallic oxides $Co_3V_2O_8$ (117.8 $m^2\ g^{-1}$). This suggests the doping of iron significantly enhances the specific surface area of trimetallic oxide, because of the existence of defect structure in the $Co_3V_2O_8$ lattice and the increase of the degree of amorphization.[30, 31, 41]

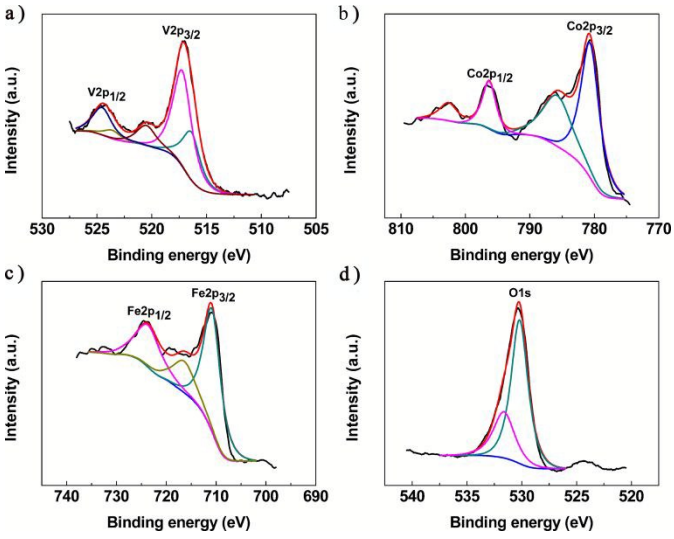

Fig2. a) V 2p, b) Co 2p, c) Fe 2p and d) O 1s XPS spectra of the V-Co-Fe-343 sample.

In order to further explore the compositions in the V-Co-Fe-343 sample, we investigate its surface elemental compositions and corresponding chemical states by X–ray photoelectron spectroscopy (XPS). The XPS characterization results of V-Co-Fe-343 sample are shown in Fig. 2a-d. The overall XPS spectra for the V-Co-Fe-343 sample (Fig. S4) reveals the presence of V, Co, Fe and O in oxide. As shown in Fig. 2a, the $2p_{3/2}$ and $2p_{1/2}$ XPS peaks for V at 517.3 eV and 524.42 eV, respectively, are observed, which indicates that the vanadium is mainly present in the $V^{(V)}$ state, and a weak peak at 516.4 eV ($2p_{3/2}$) reveals that a tiny amount of vanadium are $V^{(IV)}$ phase.[24, 42, 43] The existence of $V^{(IV)}$ phase is possibly due to the residue of vanadium source ($V^{(IV)}$ in $VOSO_4$). The XPS peaks of Co are

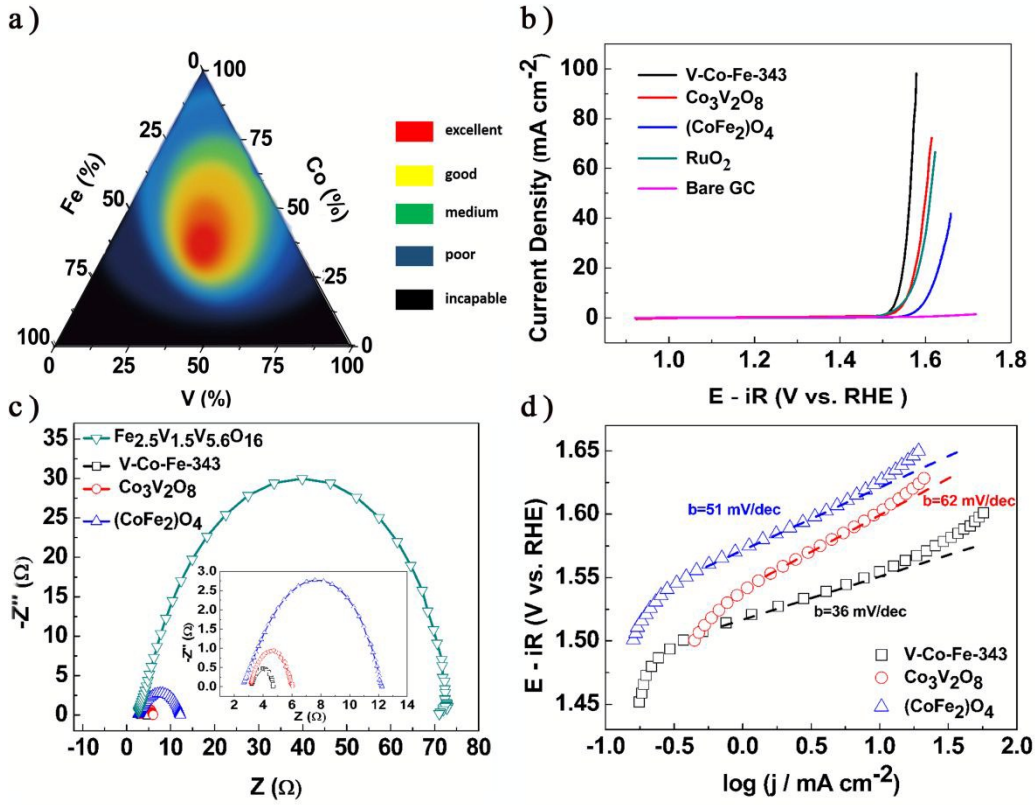

Fig3. The relationship between the molar fraction of the three metal sources and the current density at an overpotential of 400 mV are shown in this trigonal coordinate plot; The excellent (>90 mA cm^{-2}), good (60-90 mA cm^{-2}), medium (30-60 mA cm^{-2}), poor (10-30 mA cm^{-2}) and no (<10 mA cm^{-2}) catalytic activity are marked using red, yellow, green, blue and black, respectively; b) The polarization curves of $Co_3V_2O_8$, $(CoFe_2)O_4$, V-Co-Fe-343 catalysts and commercial RuO_2 at a sweep rate of 10 mV s^{-1} with a rotation speed of 1600 rpm; c) The EIS of $Co_3V_2O_8$, $(CoFe_2)O_4$, V-Co-Fe-343 and $Fe_{2.5}V_{1.5}V_{5.6}O_{16}$ catalysts at 1.70 V *vs.* RHE, respectively, on the carbon fiber paper. d) Corresponding Tafel plots.

observed at 780.9 eV ($2p_{3/2}$) and 796.4 eV ($2p_{1/2}$), and two satellite peaks locate at 785.7 eV and 802.6 eV, which corresponds to the $Co^{(II)}$ state (Fig. 2b).[24, 44] With regard to Fe, its 710.8 eV ($2p_{3/2}$) and 723.6 eV ($2p_{1/2}$) XPS peaks are observed in Fig. 2c, which is characteristic of a $Fe^{(III)}$ state.[28, 45] In addition, the detail O 1s XPS spectrum, presented in Fig. 2d, shows a strong peak at around 530.2 eV, which is aligned with the characteristic peak of O 1s for metal oxide samples.[15, 16, 28] Those results are consistent with the characterization results of XRD, and provide additional evidence for the formation of trimetallic oxide (the Fe-doped $Co_3V_2O_8$).

Based on the above characterization, we calculate the densities of states (DOS) of $Co_3V_2O_8$ and V-Co-Fe-343 sample obtained in this work. The DOS for $Co_3V_2O_8$ near the Fermi level, as shown in Fig. S5, indicates $Co_3V_2O_8$ is intrinsically metallic.[41] Comparing with $Co_3V_2O_8$, the DOS of V-Co-Fe-343 exists a peak near the Fermi level, and is obviously intense than that of $Co_3V_2O_8$. This phenomenon suggests that V-Co-Fe-343 has a greater electrical conductivity, which can be attributed to the doping of iron, because the partial DOS of iron also has a corresponding intense peak near the Fermi level (Fig. S5, inset).

On the basis of all above results, we successfully prepared the Fe-doped $Co_3V_2O_8$ (V-Co-Fe-343, Fig. 1d) nanoparticles with greate electrical conductivity and high specific surface area because of its small particle size, large degree of amorphization as well as rich porous structure. Those features can effectively promote that the active sites of material surface are exposed to the electrolyte, which is likely one of the major reasons for the V-Co-Fe-343 catalyst displaying good catalytic performance for OER.

Electrochemical measurements of those catalysts, loaded on glassy carbon (GC) electrode are carried out on a rotation disk electrode (RDE) in 1.0 M KOH electrolyte. Firstly, we study the correlation between the molar ratios of cobalt, iron and vanadium sources and the OER catalytic activity. As shown in Fig. 3a, the trigonal coordinate axes are established according to the molar fraction of the three metal sources, and different colours, used to mark different regions, indicate the OER catalytic activity of those catalysts at an overpotential of 400 mV, in the 1.0 M KOH electrolyte. As Fig. 3a shows, the monometallic and bimetallic oxides display a low catalytic activity for OER, but the ternary metal oxide, with proper molar ratios, have considerable catalytic activity. In particular, the V-Co-Fe-343 catalyst (the molar ratio of V, Co, Fe sources was 3: 4: 3) displays excellent catalytic activity for OER, which could be attributed to the formation of lattice defects resulting from iron doping. And excess iron source could replace vanadium in $Co_3V_2O_8$ lattice as much as possible to form iron-

rich V-Co-Fe-343 catalyst. Then we investigate the variation of OER performance with the reaction time at 180 ℃. As shown in Fig. S6, at less reaction time (below 22 h), the current density increases significantly with the extending of reaction time. When the reaction time exceeds more than 22 h, the current density begins to reduce progressively. In addition, the effect of mass loading of catalysts on the GC electrode is also studied in Fig. S7. It is appropriate for the loading of 0.28 mg cm^{-2} to combine catalytic activity and efficient utilization of catalysts. Therefore, we keep the molar ratio of V, Co and Fe sources at 3 : 4 : 3 to synthesis the Fe-doped $Co_3V_2O_8$ (the V-Co-Fe-343) with 22 h of reaction time, and investigate other catalytic properties with 0.28 mg cm^{-2} of a catalyst loading.

The linear sweep voltammetry (LSV) polarization curves for a series of metal oxides, synthesized by the same preparation method in this work, and commercial ruthenium oxide are shown in Fig. 3b and Fig. S8. As shown in Fig. 3b, the bare GC electrode makes almost no contribution to the catalytic activity for OER according to its small current density, which is one of the most essential measures for electrocatalytic OER activity. Comparing with the monometallic and bimetallic metal oxides catalysts prepared in this work, the V-Co-Fe-343 catalyst has the highest current density about 98.1 mA cm^{-2} at 1.58 V *vs.* RHE, which reveals its effective catalytic activity for OER. In addition, the catalytic performance of V-Co-Fe-343 is significantly higher than commercial ruthenium oxide. And, more remarkable, in comparison to others catalysts in this work and catalyst reported in existing literatures, the active V-Co-Fe-343 catalyst just requires a lower overpotential of 307 mV to achieve a current density of 10 mA cm^{-2} (Table S1), normally regarded as a basic factor related to hydrogen fuel synthesis.[46]

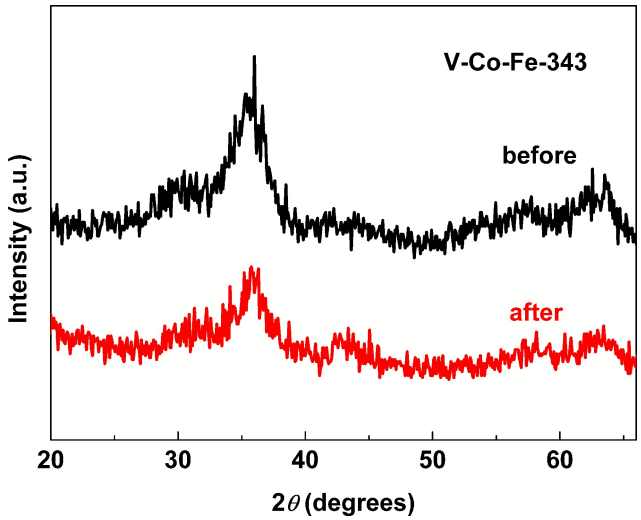

Fig4. The XRD patterns of V-Co-Fe-343 before and after 100 cycles cyclic voltammetry from 0.92 to 1.62 V vs RHE at a sweep rate of 50 mV s^{-1}.

To further study the properties of different catalysts in the electrocatalytic process, the electrochemical impedance spectroscopy (EIS) analysis is performed on a standard three-electrode system. The catalysts are loaded on carbon fiber paper and GC electrode to investigate EIS, respectively (Fig. 3c and Fig. S9). Fig. 3c records the EIS curves of $Co_3V_2O_8$, $(CoFe_2)O_4$, V-Co-Fe-343 and $Fe_{2.5}V_{1.5}V_{5.6}O_{16}$ catalysts at 1.70 V *vs.* RHE, respectively. And the charge transfer resistance (R_{ct}) for those catalysts are received by simulating the EIS data using a simplified Randles equivalent circuit (Figure S9, inset). As shown in Fig. 3c and Fig. S9, the R_{ct} of V-Co-Fe-343 catalyst is significantly lower than other catalysts in this test, which reveals its outstandingly efficient electron transport in the electrocatalytic process for the oxygen evolution reaction. This experimental result is agreed well with the above theoretical investigation (Fig. S5), which indicates that the doping of iron significantly improved the electrical conductivity of the V-Co-Fe-343 to acquire an efficient electron transport. This is an important reason the catalytic performance of the V-Co-Fe for OER is great (Fig. 3b).

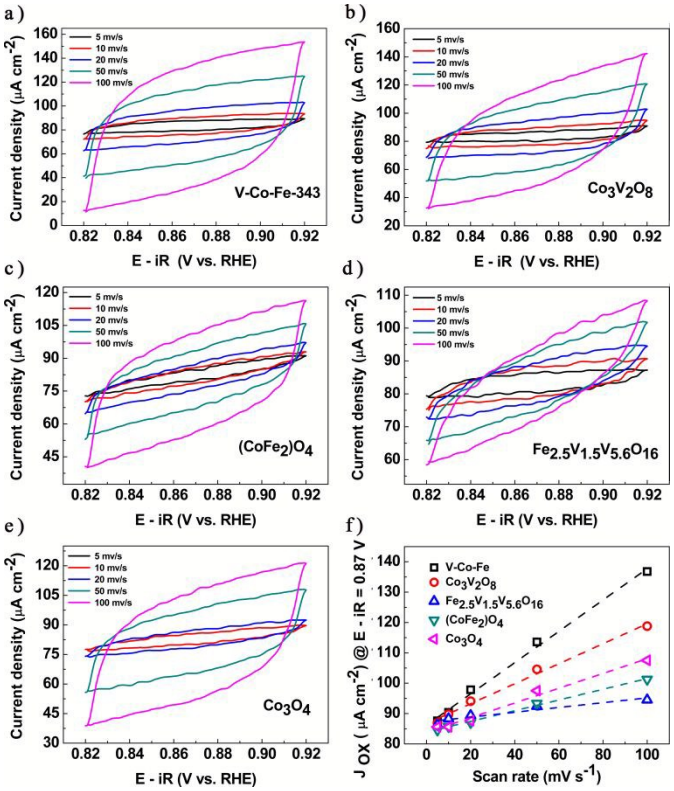

Fig5. The double-layer capacitance measurements of the obtained $Co_3V_2O_8$, $(CoFe_2)O_4$, V-Co-Fe-343, $Fe_{2.5}V_{1.5}V_{5.6}O_{16}$ and Co_3O_4; (a-e) cyclic voltammograms of those catalysts at a series of scan rates of 5, 10, 20, 50 and 100 mV s^{-1} in 1.0 M KOH electrolyte; f) linear fitting of those oxidation currents at 0.87 V *vs.* RHE of those catalysts versus scan rates.

Moreover, the Tafel slope is one of direct measures to evaluate the effect of the rate-limiting step on electrocatalytic reaction process.[47] To achieve more insight to the oxygen evolution reaction process of those catalysts, we record the linear portions at low potential (in Fig. 3d and S10) and obtain the Tafel slope according to the Tafel equation: $\eta = b \log j + a$, $\eta = E_{RHE} - 1.23$ V, where b is the Tafel slope and j is the current density.[48] As shown in Fig. 3d, the Tafel slope for V-Co-Fe-343 catalyst is just 36mV dec^{-1}, which is significantly lower than $Co_3V_2O_8$ catalyst (about 62 mV dec^{-1}), $(CoFe_2)O_4$ (about 51 mV dec^{-1}) and other catalysts (Fig. S10) synthesized in this work. This suggests that the doping of iron in V-Co-Fe-343 catalyst promotes the improvement of Tafel slope in comparison with

the $Co_3V_2O_8$ catalyst. This phenomenon is in accordance with the result of a recently report about the effect of iron in metal oxide on OER.[28] Integration of efficient electron transport and the lower Tafel slope indicate that the V-Co-Fe-343 catalyst has an extremely favourable kinetics for OER.

In order to investigate the change of morphology and composition for catalyst during oxygen evolution reaction, we compare the XRD patterns, HRTEM images and energy-dispersive X-ray spectroscopy (EDS) in the HRTEM of the V-Co-Fe-343 before and after cyclic voltammetry from 0.92 to 1.62 V vs RHE (100 cycles). As show in Fig. 4, the XRD patterns of cycled V-Co-Fe-343 become weaker for diffraction intensity and broader for peak width, comparing with that of the initial catalyst. And, the crystal lattices are unordered after cyclic voltammetry (Fig. S11). Those results all indicate the increase of degree of amorphization for the V-Co-Fe-343 during OER, which is an important reason for the improved catalytic activity.[31] In addition, the EDS show apparent increase in the content of cobalt and iron (Fig. S12), which suggests the form of more active sites (cobalt and iron oxo/hydroxide).[31, 32] Moreover, the presence of iron significantly increases the degree of amorphization and specific surface area according to Fig. 1a and Fig. S3 before OER. Those effects can promote the exposure of the catalyst surface to electrolyte and be good for the further increase of degree of amorphization to get a high OER activity.

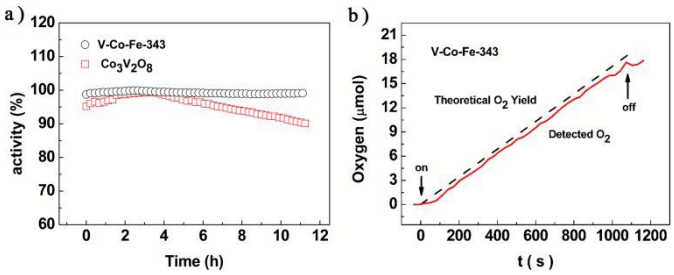

Fig6. a) The stability of $Co_3V_2O_8$ and V-Co-Fe-343 catalysts; b) The Faradaic efficiency testing of V-Co-Fe-343 catalyst for OER; in 1.0 M KOH electrolyte, at 1.55 V *vs.* RHE.

In addition, the V-Co-Fe-343 catalyst with large degree of amorphization and small particle size has a high specific surface and can provide more surface sites to catalyze oxygen evolution reaction than other catalysts in this work. Thus, we investigate the electrochemically active surface area (A_{echem}) of different catalysts, which is presented in Fig. 5. Because there is a positive correlation between the value of electrochemical double-layer capacitance (C_{dl}) and the product of A_{echem} and the scan rate (v), namely $C_{dl} \propto v \times A_{echem}$, A_{echem} can be calculated from C_{dl} of the catalytic surface.[15, 49] And linear relationship shown in Fig. 5f can be utilized to estimate C_{dl} *via* the slope.[21]

In terms of Fig. 5a-e, we can find that C_{dl} of V-Co-Fe-343 catalyst (about 589 μF cm^{-2} at a potential range of 0.82-0.92 V *vs.* RHE) is remarkably high than other catalysts (475 μF cm^{-2} for $Co_3V_2O_8$, 335 μF cm^{-2} for Co_3O_4, 307 μF cm^{-2} for $(CoFe_2)O_4$ and 273 μF cm^{-2} for $Fe_{2.5}V_{1.5}V_{5.6}O_{16}$). As expected, V-Co-Fe-343 catalyst has a larger electrochemically active surface area (A_{echem}) and can provide more active sites exposed to the electrolyte, which is compatible with the results of SEM (Fig. 1) and BET (Fig. S3).

It is well-known that the high catalytic performance and good stability are two basic peculiarity of an excellent catalyst. Only when possessing the two features at the same time, the catalysts have the potential for OER in large-scale commercial applications. The stability of the obtained V-Co-Fe-343 catalyst is tested by loading it on carbon fiber paper, using $Co_3V_2O_8$ obtained in this work for reference sample. Fig. 6a displays that the current density of V-Co-Fe-343 catalyst collapses by less than 3 percent at 1.55V *vs.* RHE after 11 h, compared to the initial value. But the current density of $Co_3V_2O_8$ catalyst drops considerably. In addition, comparing the charge transfer resistance (R_{ct}) at different potential *vs.* RHE (1.50 V, 1.55 V, 1.60 V and 1.70 V *vs.* RHE, respectively) of V-Co-Fe-343 catalyst before and after reaction (Fig. S13), we can find that even the V-Co-Fe-343 catalyst has worked a long time, it also possesses efficient electron transport for oxygen evolution reaction. Those all reveal the outstanding stability of V-Co-Fe-343 catalyst. Beyond that, the Faradaic efficiency of V-Co-Fe-343 catalyst is assessed using single-compartment device at 1.55 V *vs.* RHE, in order to verify that the current of working electrode is exclusively caused by oxygen evolution reaction. In Fig. 6b, the actual O_2 production (the red line) obtained according to the Henry's law is compared with the theoretical O_2 yield based on the current (dashed). The current efficiency of oxygen-producing is about 94%, which suggests the high-efficiency current-to-oxygen conversion.

Conclusions

In summary, Fe-doped $Co_3V_2O_8$ nanoparticles (iron-rich V-Co-Fe-343) have been successfully prepared using simple hydrothermal method, and they have effective catalytic performance for the oxygen evolution reaction in alkaline media. Because of possessing large degree of amorphization, rich porous structure and high specific surface area, the V-Co-Fe-343 catalyst can promote the exposure of the catalyst surface to electrolyte to provide more active sites for OER. The electrochemical measurements show that the current density of the V-Co-Fe-343 catalyst (about 98.1 mA cm^{-2} at 1.58 V *vs.* RHE) is significantly high than the bimetallic and monometallic oxides catalyst prepared in this work. The V-Co-Fe-343 catalyst with a small Tafel slope of 36 mV dec^{-1} just needs a lower overpotential of 307 mV to achieve a current density of 10 mA cm^{-2}. In addition, the V-Co-Fe-343 catalyst also has excellent durability, and even after an 11-hour electrocatalytic oxygen evolution reaction at 1.55V *vs.* RHE, its current density still remains to be exceeded 97% of the initial value. Moreover, this simple and convenient method to obtain polymetallic oxide nanoparticles may promote the preparation and application of complex metal oxide catalysts with high catalytic activity, low cost and green environment protection to manufacture renewable energy.

Acknowledgements

We gratefully acknowledge the financial support of this research by the National Nature Science Foundation of China (no. 21275104).

Notes and references

1 Y. Yan, B. Xia, Z. Xu and X. Wang, *ACS Catal.*, 2014, **4**, 1693-1705.
2 D. Strmcnik, M. Uchimura, C. Wang, R. Subbaraman, N. Danilovic, D. van der Vliet, A. P. Paulikas, V. R. Stamenkovic and N. M. Markovic, *Nat. Chem.*, 2013, **5**, 300-306.
3 P. Strasser, *Rev. Chem. Eng.*, 2009, **25**, 255-295.
4 Z. Y. Jin, P. P. Li, G. Y. Liu, B. Z. Zheng, H. Y. Yuan and D. Xiao, *J. Mater. Chem. A*, 2013, **1**, 14736-14743.
5 W. F. Chen, K. Sasaki, C. Ma, A. I. Frenkel, N. Marinkovic, J. T. Muckerman, Y. Zhu and R. R. Adzic, *Angew. Chem. Int. Ed.*, 2012, **51**, 6131-6135.
6 K. Kinoshita, *Electrochemical oxygen technology*, John Wiley & Sons, 1992.
7 Q. S. Yin, J. M. Tan, C. Besson, Y. V. Geletii, D. G. Musaev, A. E. Kuznetsov, Z. Luo, K. I. Hardcastle and C. L. Hill, *Science*, 2010, **328**, 342-345.
8 M. W. Kanan and D. G. Nocera, *Science*, 2008, **321**, 1072-1075.
9 H. S. Ahn and T. D. Tilley, *Adv. Funct. Mater.*, 2013, **23**, 227-233.
10 I. Katsounaros, S. Cherevko, A. R. Zeradjanin and K. J. J. Mayrhofer, *Angew. Chem. Int. Ed.*, 2014, **53**, 102-121.
11 Z. Y. Jin, P. P. Li and D. Xiao, *Sci Rep-Uk*, 2014, **4**, 6712-6718..
12 H. F. Liang, F. Meng, M. Caban-Acevedo, L. S. Li, A. Forticaux, L. C. Xiu, Z. C. Wang and S. Jin, *Nano Lett.*, 2015, **15**, 1421-1427.
13 S. Park, D. Kim, C. Lee, S.-D. Seo, H. Kim, H. Han, K. Hong and D.-W. Kim, *Nano Research*, 2014, **7**, 144-153.
14 J. Wang, H. X. Zhong, Y. L. Qin and X. B. Zhang, *Angew. Chem. Int. Ed.*, 2013, **52**, 5248-5253.
15 P. P. Li, Z. Y. Jin and D. Xiao, *J. Mater. Chem. A*, 2014, **2**, 18420-18427.
16 A. J. Esswein, M. J. McMurdo, P. N. Ross, A. T. Bell and T. D. Tilley, *J. Phys. Chem. C*, 2009, **113**, 15068-15072.
17 J. W. Lang, L. B. Kong, M. Liu, Y. C. Luo and L. Kang, *J. Electrochem. Soc.*, 2010, **157**, A1341-A1346.
18 J. Zhang, Z. Zhao, Z. Xia and L. Dai, *Nat. Nanotechnol.*, 2015, **10**, 444-452.
19 J. G. McAlpin, Y. Surendranath, M. Dinca, T. A. Stich, S. A. Stoian, W. H. Casey, D. G. Nocera and R. D. Britt, *J. Am. Chem. Soc.*, 2010, **132**, 6882-6883.
20 X. Lu, Y. H. Ng and C. Zhao, *ChemSusChem*, 2014, **7**, 82-86.
21 T. Y. Ma, S. Dai, M. Jaroniec and S. Z. Qiao, *J. Am. Chem. Soc.*, 2014, **136**, 13925-13931.
22 J. A. Haber, D. Guevarra, S. H. Jung, J. Jin and J. M. Gregoire, *Chemelectrochem*, 2014, **1**, 1613-1617.
23 N. Jiang, B. You, M. Sheng and Y. Sun, *Angew. Chem. Int. Ed.*, 2015, **54**, 6251-6254.
24 M. Xing, L.-B. Kong, M.-C. Liu, L.-Y. Liu, L. Kang and Y.-C. Luo, *J. Mater. Chem. A*, 2014, **2**, 18435-18443.
25 C. J. Gaston, K. A. Pratt, X. Y. Qin and K. A. Prather, *Environ. Sci. Technol.*, 2010, **44**, 1566-1572.
26 I. Ortiz-Bernad, R. T. Anderson, H. A. Vrionis and D. R. Lovley, *Appl. Environ. Microbiol.*, 2004, **70**, 3091-3095.
27 Y. Z. Wu, M. X. Chen, Y. Z. Han, H. X. Luo, X. J. Su, M. T. Zhang, X. H. Lin, J. L. Sun, L. Wang, L. Deng, W. Zhang and R. Cao, *Angew. Chem. Int. Ed.*, 2015, **54**, 4870-4875.
28 R. D. Smith, M. S. Prévot, R. D. Fagan, S. Trudel and C. P. Berlinguette, *J. Am. Chem. Soc.*, 2013, **135**, 11580-11586.
29 J. A. Haber, C. X. Xiang, D. Guevarra, S. H. Jung, J. Jin and J. M. Gregoire, *Chemelectrochem*, 2014, **1**, 524-528.
30 M. Bajdich, M. Garcia-Mota, A. Vojvodic, J. K. Norskov and A. T. Bell, *J. Am. Chem. Soc.*, 2013, **135**, 13521-13530.
31 K. J. May, C. E. Carlton, K. A. Stoerzinger, M. Risch, J. Suntivich, Y. L. Lee, A. Grimaud and Y. Shao-Horn, *J. Phys. Chem. Lett.*, 2012, **3**, 3264-3270.
32 M. S. Burke, M. G. Kast, L. Trotochaud, A. M. Smith and S. W. Boettcher, *JACS*, 2015, **137**, 3638-3648.
33 P. Hohenberg and W. Kohn, *Phys Rev B*, 1964, **136**, B864-B871.
34 W. Kohn and L. J. Sham, *Physical Review*, 1965, **140**, A1133-A1138.
35 S. J. Clark, M. D. Segall, C. J. Pickard, P. J. Hasnip, M. J. Probert, K. Refson and M. C. Payne, *Zeitschrift Fur Kristallographie*, 2005, **220**, 567-570.
36 J. P. Perdew, K. Burke and M. Ernzerhof, *Phys. Rev. Lett.*, 1996, **77**, 3865-3868.
37 G. L. Zhou, H. Lan, T. T. Gao and H. M. Xie, *Chem. Eng. J.*, 2014, **246**, 53-63.
38 W. J. Shan, Z. C. Feng, Z. L. Li, Z. Jing, W. J. Shen and L. Can, *J. Catal.*, 2004, **228**, 206-217.
39 S. K. Meher and G. R. Rao, *J. Phys. Chem. C*, 2011, **115**, 15646-15654.
40 M. S. Balathanigaimani, W. G. Shim, M. J. Lee, C. Kim, J. W. Lee and H. Moon, *Electrochem. Commun.*, 2008, **10**, 868-871.
41 K. Xu, P. Z. Chen, X. L. Li, Y. Tong, H. Ding, X. J. Wu, W. S. Chu, Z. M. Peng, C. Z. Wu and Y. Xie, *J. Am. Chem. Soc.*, 2015, **137**, 4119-4125.
42 D. L. Chao, X. H. Xia, J. L. Liu, Z. X. Fan, C. F. Ng, J. Y. Lin, H. Zhang, Z. X. Shen and H. J. Fan, *Adv. Mater.*, 2014, **26**, 5794-5800.
43 J. Mendialdua, R. Casanova and Y. Barbaux, *J. Electron. Spectrosc. Relat. Phenom.*, 1995, **71**, 249-261.
44 C. Z. Yuan, L. Yang, L. R. Hou, D. K. Li, L. F. Shen, F. Zhang and X. G. Zhang, *J. Solid State Electrochem.*, 2012, **16**, 1519-1525.
45 Y. Ma, C. Zhang, G. Ji and J. Y. Lee, *J. Mater. Chem.*, 2012, **22**, 7845-7850.
46 Y. Gorlin and T. F. Jaramillo, *J. Am. Chem. Soc.*, 2010, **132**, 13612-13614.
47 *Russ. J. Electrochem.*, 2002, **38**, 1364-1365.
48 S. Chen, J. J. Duan, J. R. Ran, M. Jaroniec and S. Z. Qiao, *Energy Environ. Sci.*, 2013, **6**, 3693-3699.
49 J. D. Benck, Z. B. Chen, L. Y. Kuritzky, A. J. Forman and T. F. Jaramillo, *ACS Catal.*, 2012, **2**, 1916-1923.

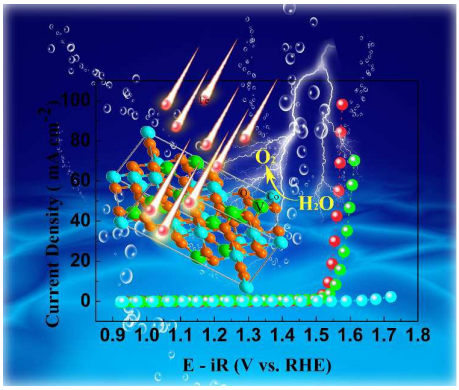

Hydrothermally synthesized V-Co-Fe oxide nanoparticles are reported as a highly active and stable electrocatalyst for oxygen evolution reaction.